Thermal applications of hybrid nanofluid containing carbon nanotubes with heat source and radiative effects

Muapper Alhadri[1], Tasawar Abbas[2], Sami Ullah Khan[3,*], Lotfi Ben Said[1], Walid Aich[1], Lioua Kolsi[1] , Huma Tayyab[2]

[1]Department of Mechanical Engineering, College of Engineering, University of Ha'il, Ha'il City 81451, Saudi Arabia

(m.alhadri@uoh.edu.sa, lo.bensaid@uoh.edu.sa, w.aich@uoh.edu.sa, l.kolsi@uoh.edu.sa)

[2]Department of Mathematics, University of Wah, Wah Cantt, 47040 Pakistan.

(tasawar.abbas@uow.edu.pk, humaq807@gmail.com)

[3,*]Department of Mathematics, Namal University Mianwali, 42250, Pakistan (samiullah@namal.edu.pk)

[*]**Corresponding author:** samiullah@namal.edu.pk (+923137141665)

Abstract: The objective of current work is to characterizes the thermal impact of carbon nanotubes due to rotating disk with applications of thermal radiation, heat source and slip effects. The single walled carbon nanotubes (SWCNTs) and multi-walled carbon nanotubes (MWCNTs) with suspension of ethylene glycol (EG) has been used to analyze the problem. The base fluid consequences are justified by using Casson fluid. The flow model is justified with interaction of velocity and thermal slip effects. Thermal characteristics of SWCNT and MWCNTs along ethylene glycol (EG) base materials has been presented. The heat transfer investigation is based on implementation of Cattaneo-Christov approach. Numerical computations are performed with help of shooting scheme. Comparative thermal analysis is performed for traditional nanofluid (SWCNT/EG) hybrid nanofluid (SWCNTs-MWCNTs/EG). Physical visualization of results for enhancement of heat transfer phenomenon is performed. It has been observed that heat transfer phenomenon is more exclusive for hybrid nanofluid (SWCNTs-MWCNTs/EG) as compared to nanofluid (SWCNT/EG. The thermal profile enhances for Casson fluid parameter.

Keywords: Heat transfer, carbon nanotubes, ethylene glycol, rotating disk, slip effects.

1. Introduction

The hybrid nanomaterials are the modified class of nanofluid having efficient thermal properties. The hybrid nanofluid represents the joint suspension of two distinct nanoparticles with base fluid. The interaction of two different nanoparticles show more strengthened thermal performances as compared to common nanofluids. Owing to high thermal impact, the hybrid nanofluids offer various kind of applications in refrigeration, nuclear systems, heat exchangers, chemical reactions, aircrafts, thermal reservoirs etc. Researchers performed various investigations for studying the hybrid nanofluid thermal impact. For instance, Sundar et al. [1] focused to investigating the thermal interpretation of hybrid nanofluid under the influence of different friction sources. Ahmad et al. [2] addressed the heat transfer impact due to graphene oxide and sliver nanoparticles in order to evaluates the boosted performances of kerosene oil base liquid. Ali et al. [3] predicted the thermo-fluid apsects of hybrid nanofluid due to couette channel. Faridi et al. [4] predicted the heat fluctuation due to hybrid nanofluid due to stretched surface flow. Analysis highlighting the thermal reservations of carbon nanotubes confined to curved surface was elaborated by Abideen and Saif [5]. Oudina et al. [6] visualized the hydromagnetic flow of magnetite nanoparticles to improve the heat transfer phenomenon. Borode et al. [7] worked out artificial neural network analysis for describing the thermo-physical of hybrid nanofluid via experimental approach. Malika et al. [8] deduced the thermal simulations based on hybrid nanofluid flow with significance to heat exchangers. Titanium oxide and silica nanoparticles were used to improve the thermal prospective of water base fluid. Alawi et al. [9] described the solar collectors applications due to utilization of hybrid nanomaterial. The results were supported with machine learning algorithms. Squeezing flow of copper oxide and aluminum nanoparticles for Darcy-Forchheimer applications has been analyzed by Hayat et al. [10]. Acharya et al. [11] presents the investigation for energy storage due to semi-circular flow of hybrid nanofluid. Srilatha et al. [12] studied the machine learning analysis for interface layer of hybrid nanofluid due to porous disk. Foukhari et al. [13] performed evaluation of entropy production due to hybrid nanofluid due to two coaxial porous cylinders. Sarfraz and Khan [14] claimed the heat transfer improvement with interaction of hybrid nanofluid in wedge shaped surface. Mahboobtosi et al. [15] utilized the entropy generation effects in curved surface flow comprising the hybrid nanofluid. Rostami et al. [16] studied the thermal outcomes for dust particles with mixture of hybrid nanofluid. Zangooee et al. [17] used the interference of slip to inspect the diverse thermal mechanism of hybrid nanofluid. Hosseinzadeh et al. [18] performed the heat transfer computations based on iron oxide and molybdenum disulfide nanoparticles in

sinusoidal cylinder. Comparative thermal observations for The thermal evaluation associated to concave parabolic, trapezoidal and convex cross configurations with utilization of hybrid nanofluid has been inspected by Hosseinzadeh et al. [19]. Paul et al. [20] depicted the contribution of Casson hybrid nanofluid governed by exponentially stretched cylinder. Investigation for improvement of heat fluctuation in vertically driven flow of hybrid nanofluid was proposed by Paul et al. [21]. Sarma and Paul [22] analyzed the bioconvective achievement for decomposition of hybrid nanoparticles. Copper oxide and gold nanoparticles were used to investigate the thermal phenomenon. The heat fluctuation due to ternary hybrid nanofluid in rotating disk was visualized by Paul et al. [23]. In another investigation, Paul et al. [24] utilized the Hall effects in Casson hybrid nanofluid flow with fluctuation of heat transfer.

In above cited research work, it has been noticed that various studies are performed for analyzing the heat transfer due to hybrid nanofluid. However, comparative thermal observations for nanofluid and hybrid nanomaterial due to rotating disk with slip effects is not focused yet. Therefore, objective of current work is to study comparative thermal analysis due to radiative flow of hybrid nanofluid with applications of slip effects and external heat source. The hybrid nanofluid is based on interaction of single walled carbon nanotubes (SWCNTs) and multi-walled carbon nanotubes (MWCNTs) with ethylene glycol (EG) base fluid. Comparative thermal simulations are addressed for traditional nanofluid (SWCNTs/EG) and hybrid nanofluids (SWCNTs-MWCNTs/EG). The novel aspects of this investigation are:

- A suspension of single walled carbon nanotubes (SWCNTs) and multi-walled carbon nanotubes (MWCNTs) with ethylene glycol due to rotating disk have been considered.
- The base fluid properties are highlighted by Casson fluid model.
- The investigation is subject to velocity and thermal slip constraints.
- Heat transfer model is updated with implementation of Cattaneo-Christov theory.
- Numerical computations associated to flow problem are performed with shooting scheme.
- Comparative analysis is performed for prediction of heat transfer is addressed for traditional nanofluid (SWCNTs/EG) and hybrid nanofluids (SWCNTs-MWCNTs/EG).

2. Formulation of problem

Let us observe the heat transfer analysis due to interaction of single walled carbon nanotubes (SWCNTs) and multi-walled carbon nanotubes (MWCNTs) with ethylene glycol base liquid. The flow problem is modeled in view of following flow assumptions:

- Assuming a steady flow transport of ethylene glycol base fluid with suspension of single walled carbon nanotubes (SWCNTs) and multi-walled carbon nanotubes (MWCNTs).
- The rotatory disk accounted the flow as shown in Fig. 1.
- For development of mathematical model, the cylindrical coordinates are used with coordinates r,θ and z. Denoting velocity components with v_r, v_θ and v_z.
- The rotation of disk is considered along z-direction maintain angular velocity Ω.
- Slip effects for both temperature and velocity profile have been considered [25].
- The heat source and radiation significance for inspection of heat transfer is considered.
- The upgraded energy equation is used with implication of modified Fourier law.

The governing equations for stated flow constraints are expressed as [5, 25]:

$$\frac{\partial v_r}{\partial r}+\frac{v_r}{r}+\frac{\partial v_z}{\partial z}=0, \tag{1}$$

$$\rho_{hnf}\left(v_r\frac{\partial v_r}{\partial r}+v_z\frac{\partial v_r}{\partial z}-\frac{{v_\theta}^2}{r}\right)=\mu_{hnf}\left(1+\frac{1}{\gamma}\right)\left(\frac{\partial^2 v_r}{\partial r^2}+\frac{1}{r}\frac{\partial v_r}{\partial r}+\frac{\partial^2 v_r}{\partial z^2}-\frac{v_r}{r^2}\right)-\sigma_{hnf}{B_0}^2 v_r, \tag{2}$$

$$\rho_{hnf}\left(v_r\frac{\partial v_\theta}{\partial r}+v_z\frac{\partial v_\theta}{\partial z}-\frac{v_r v_\theta}{r}\right)=\mu_{hnf}\left(1+\frac{1}{\gamma}\right)\left(\frac{\partial^2 v_\theta}{\partial r^2}+\frac{1}{r}\frac{\partial v_\theta}{\partial r}+\frac{\partial^2 v_\theta}{\partial z^2}-\frac{v_\theta}{r^2}\right)-\sigma_{hnf}{B_0}^2 v_\theta, \tag{3}$$

$$\rho_{hnf}\left(v_r\frac{\partial v_z}{\partial r}+v_z\frac{\partial v_z}{\partial z}\right)=\mu_{hnf}\left(1+\frac{1}{\gamma}\right)\left(\frac{\partial^2 v_z}{\partial r^2}+\frac{1}{r}\frac{\partial v_z}{\partial r}+\frac{\partial^2 v_z}{\partial z^2}\right), \tag{4}$$

$$\begin{aligned} &v_r\frac{\partial T}{\partial r}+v_z\frac{\partial T}{\partial z}=\alpha_{hnf}\left(\frac{\partial^2 T}{\partial r^2}+\frac{1}{r}\frac{\partial T}{\partial r}+\frac{\partial^2 T}{\partial z^2}\right)-\frac{16}{3}\frac{\sigma^* {T_\infty}^3}{k^*\left(\rho c_p\right)_{hnf}}\left(\frac{\partial^2 T}{\partial r^2}+\frac{1}{r}\frac{\partial T}{\partial r}+\frac{\partial^2 T}{\partial z^2}\right)\\ &-\lambda_t\left[{v_r}^2\frac{\partial^2 T}{\partial r^2}+{v_z}^2\frac{\partial^2 T}{\partial z^2}+2v_r v_z\frac{\partial^2 T}{\partial r\partial z}+\left(v_r\frac{\partial v_r}{\partial r}+v_z\frac{\partial v_r}{\partial z}\right)\frac{\partial T}{\partial r}+\left(v_r\frac{\partial v_z}{\partial r}+v_z\frac{\partial v_z}{\partial z}\right)\frac{\partial T}{\partial z}\right]\\ &-\frac{Q_0}{\left(\rho c_p\right)_{hnf}}\left(T-T_\infty\right), \end{aligned} \tag{5}$$

with boundary conditions [2]:

$$v_r = rs + L_0\left(1+\frac{1}{\gamma}\right)\frac{\partial v_r}{\partial z}, v_\theta = r\Omega + L_0\left(1+\frac{1}{\gamma}\right)\frac{\partial v_\theta}{\partial z}, v_z = 0, T = T_w + N_0\frac{\partial T}{\partial z},\ at\ \ z = 0. \tag{6}$$

$$v_r \to 0, v_\theta \to 0, T \to T_\infty \quad as \quad z \to \infty. \tag{7}$$

with μ_{hnf} (dynamic viscosity of hybrid nanoparticles), T_w (surface temperature), γ (Casson fluid coefficient), B_0 (magnetic field strength), $\left(\rho C_p\right)_{hnf}$ (heat capacitance), T (fluid temperature), L_0 (velocity slip coefficient), N_0 (thermal slip coefficient), ρ_{hnf} (hybrid nanofluid density), λ_t (thermal relaxation time), σ^* (Stefan Boltzmann constant), T_∞ (free stream temperature), α_{hnf} (thermal diffusivity), Q_0 (external heat source coefficient) and k^* (absorption coefficient). Numerical values for various thermal properties of SWCNTs-MWCNTs/EG suspension have been expressed in table 1.

To transform the problem into dimensionless form, following similarity transformations are suggested [5, 25]:

$$v_r = r\Omega f'(\zeta), v_\theta = r\Omega h(\zeta), v_z = -\left(2\Omega\upsilon_f\right)^{1/2} f(\zeta), \theta(\zeta) = \frac{T-T_\infty}{T_w-T_\infty}, \zeta = z\left(\frac{2\Omega}{\nu_f}\right)^{1/2}, \tag{8}$$

The dimensionless form is:

$$2\left(1+\frac{1}{\gamma}\right)f''' - \zeta_1\left[f'^2 - 2ff'' - h^2 + \zeta_2 Mf'\right] = 0, \tag{9}$$

$$2\left(1+\frac{1}{\gamma}\right)h'' + \zeta_1\left[2fh' - 2f'h - \zeta_3 Mh\right] = 0, \tag{10}$$

$$\left(\zeta_4 + Rd\right)\theta'' + \Pr Q\theta + \zeta_2 \Pr\left[f\theta' - \alpha\left(f^2\theta'' + ff'\theta'\right)\right] = 0, \tag{11}$$

And boundary conditions are given below

$$f(0) = 0, f'(0) = A + \left(1+\frac{1}{\gamma}\right)\delta f''(0), h(0) = 1 + \left(1+\frac{1}{\gamma}\right)\delta f'(0), \tag{12}$$

$$\theta(0)=1+\beta\theta'(0),\ f'(\infty)=h(\infty)=\theta(\infty)\to 0. \tag{13}$$

where M (Hartmann constant), $\Pr$ (Prandtl constant), α (thermal relaxation coefficient), A (stretching constant), δ (velocity slip parameter) and β (thermal slip parameter), Rd (thermal radiation) and Q (heat generation) which are defined as:

$$M=\sigma_f\frac{B_0^{\,2}}{\rho_f}\Omega,\ \Pr=\frac{\nu_f}{\alpha_f},\ \alpha=2\lambda_t\Omega,\ A=\frac{s}{\Omega},\ \delta=L_0\left(\frac{2\Omega}{\nu_f}\right)^{1/2},\ \beta=N_0\left(\frac{2\Omega}{\nu_f}\right)^{1/2},\ Rd=\frac{4}{3}\frac{\sigma^*T_\infty^{\,3}}{k^*k_f},$$

$$Q=\frac{Q_0}{\left(\rho c_p\right)_{hnf}}.$$

Thermo-physical constants involved in the transformed equations are defined as:

$$\zeta_1=\left(1-\phi1\right)^{2.5}\left(1-\phi2\right)^{2.5}\left[\left(1-\phi2\right)\left\{\left(1-\phi1\right)+\phi1\frac{\rho_{s1}}{\rho_f}\right\}+\phi2\frac{\rho_{s2}}{\rho_f}\right], \tag{14}$$

$$\zeta_2=\left(1-\phi1\right)^{2.5}\left(1-\phi2\right)^{2.5}\frac{\sigma_{hnf}}{\sigma_f}, \tag{15}$$

$$\zeta_3=\left[\left(1-\phi2\right)\left\{\left(1-\phi1\right)+\phi1\frac{\left(\rho c_p\right)_{s1}}{\left(\rho c_p\right)_f}\right\}+\phi2\frac{\left(\rho c_p\right)_{s2}}{\left(\rho c_p\right)_f}\right], \tag{16}$$

$$\zeta_4=\frac{k_{hnf}}{k_f}=\left[\frac{\left(k_{s2}+2k_{nf}\right)-2\phi1\left(k_{nf}-2k_{s2}\right)}{\left(k_{s2}+2k_{nf}\right)+\phi1\left(k_{nf}-2k_{s2}\right)}\right]\times\left[\frac{\left(k_{s1}+2k_f\right)-2\phi2\left(k_f-k_{s1}\right)}{\left(k_{s1}+2k_f\right)+\phi2\left(k_f-k_{s1}\right)}\right]. \tag{17}$$

where $\phi1$ defines the solid volume fractions of SWCNTs while $\phi2$ be the volume fractions of MWCNTs. The mathematical expressions for hybrid nanofluid (SWCNTs-MWCNTs/EG) and nanofluid (SWCNTs/EG) are presented in table 2.

Physical quantities skin friction and Nusselt number are defined by:

$$C_f=\frac{\tau_w}{\rho\left(\Omega r\right)^2},\ \tau_w=\mu_{hnf}\left(\frac{\partial u}{\partial y}\right)_{z=0},\ Nu_x=\frac{rq_w}{k_f\left(T_w-T_\infty\right)},\ q_w=-k_{hnf}\left(\frac{\partial T}{\partial r}\right)_{z=0} \tag{18}$$

$$\left(\mathrm{Re}_r\right)^{1/2} C_f = \frac{\left(1+\frac{1}{r}\right)}{\left(1-\phi_1\right)^{2.5}\left(1-\phi_2\right)^{2.5}} f''(0), \tag{19}$$

$$\left(\mathrm{Re}_r\right)^{-1/2} Nu_r = -\left(\frac{k_{hnf}}{k_f}\right)\theta'(0). \tag{20}$$

where $\mathrm{Re}_r = \frac{(\Omega r) r}{\upsilon_f}$ is the local Reynolds number.

3. Numerical computations

This section incorporates the implementation of shooting scheme for set of modeled equations. For initiating the simulations, the higher order system is first renovated into first order system with help of following transformations:

$$\left(s_1, s_2, s_3, s_4, s_5, s_6, s_7\right) = \left(f, f', f'', h, h', \theta, \theta'\right), \tag{21}$$

$$\begin{pmatrix} s_1' \\ s_2' \\ s_3' \\ s_4' \\ s_5' \\ s_6' \\ s_7' \end{pmatrix} = \begin{pmatrix} s_2 \\ s \\ \frac{\zeta_1\left(s_2{}^2 - 2s_1 s_3 - s_4{}^2 + \zeta_2 M s_2\right)}{2\left(1+\frac{1}{r}\right)} \\ S_5 \\ \frac{-\zeta_1}{2\left(1+\frac{1}{r}\right)}\left[2s_1 s_5 - 2s_2 s_4 - \zeta_2 M s_4\right] \\ S_7 \\ \frac{1}{\left(\left(\zeta_4 + Rd\right) - \mathrm{Pr}\,\alpha s_1{}^2\right)}\left[\zeta_3 \,\mathrm{Pr}\, s_1 s_7\left(\alpha s_2 - 1\right) - \mathrm{Pr}\, Q s_6\right] \end{pmatrix}, \tag{22}$$

The boundary conditions are reduced to:

$$\begin{pmatrix} s_1(0) \\ s_2(0) \\ s_3(0) \\ s_4(0) \\ s_5(0) \\ s_6(0) \\ s_7(0) \end{pmatrix} = \begin{pmatrix} 0 \\ A+\left(1+\frac{1}{r}\right)\delta s_1 \\ s_1 \\ 1+\left(1+\frac{1}{r}\right)\delta s_2(0) \\ s_2 \\ 1+\beta s_3 \\ s_4 \end{pmatrix}, \tag{23}$$

4. Validation of results

The simulated numerical data has been confirmed with investigation of Mustafa [26]. Table 3 shows that current numerical results claim fine accuracy with Mustafa [26].

5. Results and discussion

Physical interpretation of results has been visualized in this section. Comparative results are prepared to both nanofluid (SWCNTs/EG) and hybrid nanofluids (SWCNTs-MWCNTs/EG) with variation of modeled parameters. Fig. 2 interprets the contribution of stretching constant A on radial velocity f'. With arising numeric values, the radial velocity enhances for both fluids. The enhancement in f' is more prominent for SWCNTs-MWCNTs/EG decomposition. Fig. 3 helps to visualize the significance of velocity slip parameter δ on f' for both SWCNTs/EG and SWCNTs-MWCNTs/EG suspensions. Leading values of δ slower down the velocity for both decompositions. The momentum boundary layer also become thinner with leading variation of δ The physical description discussed in Fig. 4 announced the truncated profile of f' upon increasing Hartmann number M. The velocity profile gets compressed due to M. Physically, for peak values of M leads to interpretation of Lorentz force which slower down the velocity. Furthermore, low velocity profile is more progressive for SWCNTs/EG suspension.

Fig. 5 explains the role of thermal relaxation factor α on temperature profile θ. The temperature field gets decrement for prominent values of α. The thermal observations are deduced by varying α for SWCNTs-MWCNTs/EG and SWCNTs/EG decomposition. Physically, enhancing values of α is associated to time necessitated for fluid to maintains the original position. The reduction in θ is protuberant for SWCNTs-MWCNTs/EG. The results for observations of thermal profile

due to Casson fluid parameter γ has been predicted in Fig. 6. The temperature profile θ increases due to γ. However, magnitude of enhancement of θ is slower. Moreover, the heat transfer improvement is superior for hybrid nanofluid (SWCNTs-MWCNTs/EG). Fig. 7 presented comparative results for heat transfer subject to Casson fluid $(\phi_1 = \phi_2 = 0)$, SWCNTs/EG $(\phi_1 = 0.1, \phi_2 = 0)$ MWCNTs/EG $(\phi_1 = 0, \phi_2 = 0.1)$ and SWCNTs-MWCNTs/EG $(\phi_1 = \phi_2 = 0.1)$. Heat transfer fluctuation is more slower for Casson fluid while improved results for thermal profile is associated $(\phi_1 = \phi_2 = 0.1)$ Fig. 8 aims to understand the behavior of θ in view of nanoparticles volume fraction ϕ_1 and ϕ_2. Comparative observations are revealed for SWCNTs /EG and SWCNTs-MWCNTs/EG. Figure clearly indicating that θ enriches for variation of ϕ_1 and ϕ_2. The improvement in heat transfer is maximum for SWCNTs-MWCNTs/EG as compared to SWCNTs /EG. In Fig. 9, the results for influence of Prandtl number Pr are addressed against θ. Larger change to Pr pronounced lower heat transfer for nanofluid and hybrid nanofluid. Physically, larger values of Pr corresponds to low mass diffusivity due to which θ shows retarded trend. In order to execute the performances of heat source Q on θ Fig. 10 have been prepared. An increasing variation with larger Q is exhibited on profile of θ. The presence of heat source provides extra energy to the system which boosted the temperature profile. Fig. 11 reflects the analysis for radiation parameter Rd on θ. Change in Rd leads to boost the temperature profile for both SWCNTs-MWCNTs/EG and SWCNTs/EG. The radiation phenomenon is associated to transfer of energy through electromagnetic waves.

5. Conclusions

The heat transfer analysis with utilization of single walled and multi-walled carbon nanofluid with ethylene glycol base fluid have been performed due to rotating disk. The significance of heat and radiative phenomenon are addressed. The Cattaneo-Christov heat flux model is used to modify the heat equation. Comparative thermal observations for nanofluid (SWCNTs/EG) and hybrid nanofluid (SWCNTs-MWCNTs/EG) are investigated. Major results are summarized as:

- The radial velocity enhances due to stretching parameter for nanofluid and hybrid nanofluid. However, interaction of slip leads to reduction of velocity profile.

- Change in thermal relaxation parameter leads to decrement of temperature profile for both SWCNTs/EG and SWCNTs-MWCNTs/EG suspensions.
- The heat transfer enhances for Casson fluid parameter. The improvement in thermal profile is prominent for hybrid nanofluid.
- The fluctuation in heat transfer is more exclusive for hybrid nanofluid as compared to traditional nanofluid.
- Subject to increasing heat source and radiation parameter, temperature profile boosted.
- The heat transfer phenomenon increases for nanoparticles volume fraction of single walled carbon nanotubes (SWCNTs) and multi-walled carbon nanotubes (MWCNTs). However, the improvement in thermal profile is dominant for MWCNTs.
- The modification in current results can be suggested by studying the entropy generation analysis, bioconvection phenomenon and stability analysis.

Acknowledgment:

This research has been funded by Scientific Research Deanship at University of Ha'il, Saudi Arabia through project number RG-24 028.

Reference

[1]. Sundar, L. S., Sharma, K. V. Singh, M. K., et al. "Hybrid nanofluids preparation, thermal properties, heat transfer and friction factor –A review," *Renew. Sustain. Energy Rev.*, **68**, pp. 185–198 (2017). DOI: https://doi.org/10.1016/j.rser.2016.09.108.

[2]. Ahmad, F., Abdal, S., Ayed, H., et al., "The improved thermal efficiency of Maxwell hybrid nanofluid comprising of graphene oxide plus silver / kerosene oil over stretching sheet", *Case Stud Therm. Eng.* **27** pp. 101257 (2021). DOI: https://doi.org/10.1016/j.csite.2021.101257.

[3]. Ali, K., Reddy, Y. R., Shekar, B. C., "Thermo-fluidic transport process in magnetohydrodynamic couette channel containing hybrid nanofluid", *Partial Diff. Eqs. Appl. Math.* **7,** pp. 100468 (2023), DOI: https://doi.org/10.1016/j.padiff.2022.100468.

[4]. Faridi, A. A., Khan, N., Ali, K., "A novel numerical note on the enhanced thermal features of water-ethylene glycol mixture due to hybrid nanoparticles (MnZnFe2O4 – Ag) over a

magnetized stretching surface", *Numer. Heat Transf. B*, 1–23 (2023). DOI: https://doi.org/10.1080/10407790.2023.2296082.

[5]. Abideen, Z. U., Saif, R. S., "Impact of thermal radiation and internal heat generation on Casson nano-fluid flowing by a curved stretchable surface with suspension of carbon nanotubes (CNTs)", *Heliyon*, **9(8)**, pp. e18941 (2023). DOI: https://doi.org/10.1016/j.heliyon.2023.e18941.

[6]. Mebarek-Oudina, F., Preeti, A. S. Sabu et al. "Hydromagnetic flow of magnetite–water nanofluid utilizing adapted Buongiorno model", *Int. J. Modern Phys. B*, **38(01)**, pp. 2450003 (2024). DOI: https://doi.org/10.1142/S0217979224500036.

[7]. Adeola, B., Tshephe, T., Olubambi, P., et al, "Effects of temperature and nanoparticle mixing ratio on the thermophysical properties of GNP–Fe2O3 hybrid nanofluids: an experimental study with RSM and ANN modeling", *J. Therm. Anal. Calor.*, **149**, pp. 5059-5083 (2024). DOI:https://doi.org/10.1007/s10973-024-13029-3.

[8]. Manjakuppam, M., Sonawane, S. S., "Ecological optimization and LCA of TiO2-SiC/water hybrid nanofluid in a shell and tube heat exchanger by ANN", *Proc. Inst. Mech. Eng. E.*, **238(1)**, pp. 45-55 (2024). DOI: https://doi.org/10.1177/09544089221093304.

[9]. Alawi, O. A., Kamar, H. M., Ali, H., et al., "Design optimization of solar collectors with hybrid nanofluids: An integrated ansys and machine learning study", *Solar Energy Materials and Solar Cells*, **271**, 112822 (2024). DOI: https://doi.org/10.1016/j.solmat.2024.112822.

[10]. Hayat, T., A. Fatima and Muhammad, K., "Heat transfer and entropy analysis in squeezing flow of hybrid nanofluid (Au-CuO/NaAlg) with DF (Darcy-Forchheimer) and CC (Cattaneo-Christov) heat flux", *Mater. Sci. Eng. B*, 288, pp. 116150 (2023). DOI: https://doi.org/10.1016/j.mseb.2022.116150.

[11]. Acharya, N, and Öztop, H. F., "On the entropy analysis and hydrothermal behavior of buoyancy-driven magnetized hybrid nanofluid flow within a semi-circular chamber fitted with a triangular heater: application to thermal energy storage for energy management", *Numer. Heat Transf. A.*, pp. 1-31 (2023). DOI: https://doi.org/10.1080/10407782.2023.2281541.

[12]. Pudhari, S., Gowda, R. J. P., Madhu, J. et al., "Designing a solid–fluid interface layer and artificial neural network in a nanofluid flow due to rotating rough and porous

disk", *J. Therm. Anal. Calor.*, **149(2)**, pp. 867-878 (2024). DOI: https://doi.org/10.1007/s10973-023-12706-z

[13]. Foukhari, Y., M. Sammouda, and M. Driouich. "Entropy generation analysis of hybrid-nanofluid during natural convection through two coaxial cylinders partially filled with porous medium under magnetic field", *Sci. Iran.* (2024). DOI: 10.24200/SCI.2024.62997.8159.

[14]. Mahnoor, S., and Khan, M., "Energy optimization of water-based hybrid nanomaterials over a wedge-shaped channel", *Sci. Iran.* **31(1)**, pp. 71-82 (2024). DOI: 10.24200/SCI.2023.60254.6689.

[15]. Mehdi, M., Hosseinzadeh, Kh., and Ganji, D. D., "Entropy generation analysis and hydrothermal optimization of ternary hybrid nanofluid flow suspended in polymer over curved stretching surface", *Int. J. Thermofluids*, **20**, pp. 100507 (2023). DOI: https://doi.org/10.1016/j.ijft.2023.100507.

[16]. Rostami, T., Najafabadi, H., M. F., Hosseinzadeh, Kh., et al., "Investigation of mixture-based dusty hybrid nanofluid flow in porous media affected by magnetic field using RBF method", *Int. J. Amb. Energy*, **43(1)**, pp. 6425-6435 (2022). DOI: https://doi.org/10.1080/01430750.2021.2023041

[17]. Zangooee, M. R., Hosseinzadeh, Kh., and Ganji, D. D., "Hydrothermal analysis of hybrid nanofluid flow on a vertical plate by considering slip condition", *Theor. Appl. Mech. Lett.*,**12(5)**, pp. 100357 (2022). DOI: https://doi.org/10.1016/j.taml.2022.100357.

[18]. Hosseinzadeh, Kh, Mardani, M. R., Salehi, S., et al., "Investigation of micropolar hybrid nanofluid (iron oxide–molybdenum disulfide) flow across a sinusoidal cylinder in presence of magnetic field", *Int. J. Appl. Comput. Math.* **7**, pp. 1-17 (2021). DO: https://doi.org/10.1007/s40819-021-01148-6

[19]. Hosseinzadeh, S., Hosseinzadeh, Kh., Hasibi, A. et al., "Thermal analysis of moving porous fin wetted by hybrid nanofluid with trapezoidal, concave parabolic and convex cross sections", *Case Stud. Therm. Eng.* **30**, pp. 101757 (2022). DOI: https://doi.org/10.1016/j.csite.2022.101757.

[20]. Paul, A., Das, T. K., Nath, J. M., "Numerical investigation on the thermal transportation of MHD Cu/Al 2 O 3-H 2 O Casson-hybrid-nanofluid flow across an

exponentially stretching cylinder incorporating heat source", *Phys. Scr*. **97(8)**, pp. 085701 (2022). DOI: 10.1088/1402-4896/ac7981.

[21]. Paul, A., Das, T. K., Nath, J. M., "Thermally stratified Cu–Al2O3/water hybrid nanofluid flow with the impact of an inclined magnetic field, viscous dissipation and heat source/sink across a vertically stretching cylinder", *Zeitschrift für Angewandte Mathematik und Mechanik,* **104(2)**, pp. e202300084 (2024). DOI: https://doi.org/10.1002/zamm.202300084.

[22]. Sarma, N., and Paul, A., "Thermophoresis and brownian motion influenced bioconvective cylindrical shaped ag–cuo/h2o ellis hybrid nanofluid flow along a radiative stretched tube with inclined magnetic field", *BioNanoScience,* **14(2)**, pp. 1266-1292 (2024). DOI: https://doi.org/10.1007/s12668-023-01280-1.

[23]. Paul, A., Patgiri, B., and Sarma, N., "Darcy-Forchheimer flow of Ag–ZnO–CoFe2O4/H2O Casson ternary hybrid nanofluid induced by a rotatory disk with EMHD", *Int. J. Amb. Energy*, **45(1)**, pp. 2313697 (2024). DOI: https://doi.org/10.1080/01430750.2024.2313697

[24]. Paul, A., Patgiri, B., and Sarma, N., "Transformer oil-based Casson ternary hybrid nanofluid flow configured by a porous rotating disk with hall current, *Zeitschrift für Angewandte Mathematik und Mechanik,* **104(4)**, pp. e202300704 (2024). DOI: https://doi.org/10.1002/zamm.202300704.

[25]. Puneet R., Mackolil, J., Mahanthesh, B., Muhammad, T., "Cattaneo-Christov Theory to model heat flux effect on nanoliquid slip flow over a spinning disk with nanoparticle aggregation and Hall current", 2022. *Waves Random Complex Media*, DOI: 10.1080/17455030.2022.2048127

[26]. Mustafa, M., "MHD nanofluid flow over a rotating disk with partial slip effects: Buongiorno model", *Int. J. Heat Mass Tran.* **108,** pp. 1910–1916 (2017). DOI: https://doi.org/10.1016/j.ijheatmasstransfer.2017.01.064.

Figure and table captions

Fig. 1: Illustration of flow problem

Fig. 2: Velocity profile f' for A.

Fig. 3: Velocity profile f' for δ.

Fig. 4: Velocity profile f' for M.

Fig. 5: Temperature profile θ for α.

Fig. 6: Temperature profile θ for γ.

Fig. 7: Temperature profile θ for Casson fluid, Casson nanofluid and Casson hybrid nanofluid.

Fig. 8: Temperature profile θ for ϕ_1, ϕ_2.

Fig. 9: Temperature profile θ for Pr.

Fig. 10: Temperature profile θ for Q.

Fig. 11: Temperature profile θ for Rd.

Table 1: Thermal properties SWCNTs and MWCNTs with ethylene glycol base liquid.

Table 2. Thermo-physical features of nanofluid (SWCNTs/EG) and hybrid nanofluids (SWCNTs-MWCNTs/EG) [5].

Table 3: Comparison of numerical results with study of Mustafa [26] taking $A = 0,\ \phi_1 = \phi_2 = 1$ and $\gamma \to \infty$.

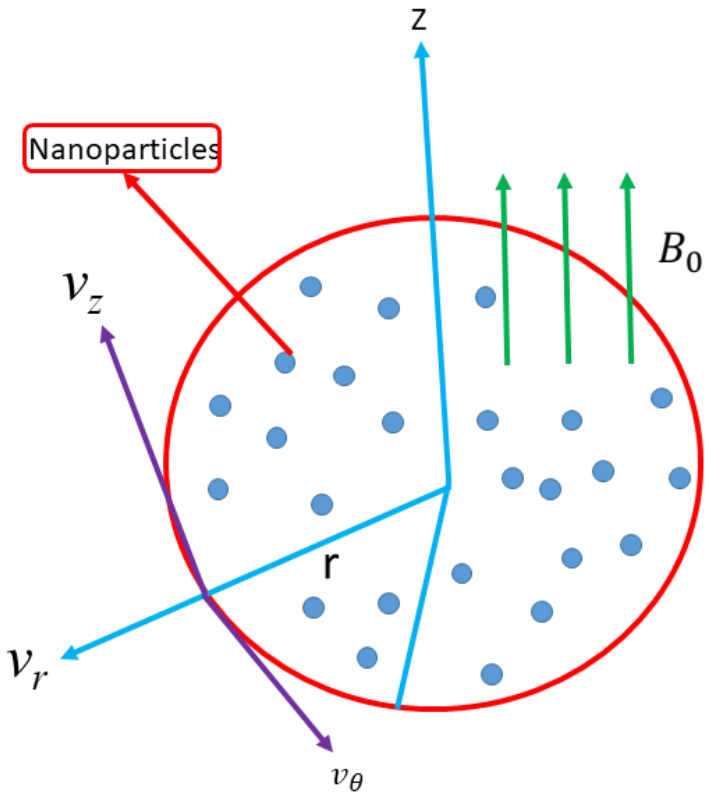

Fig. 1: Illustration of flow problem.

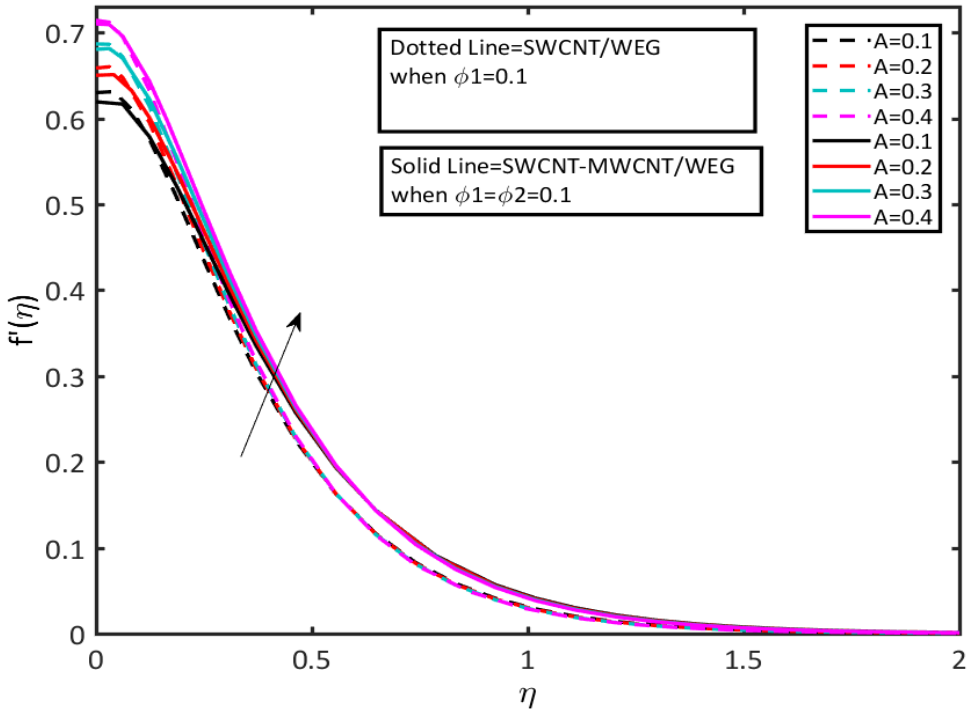

Fig. 2: Velocity profile f' for A.

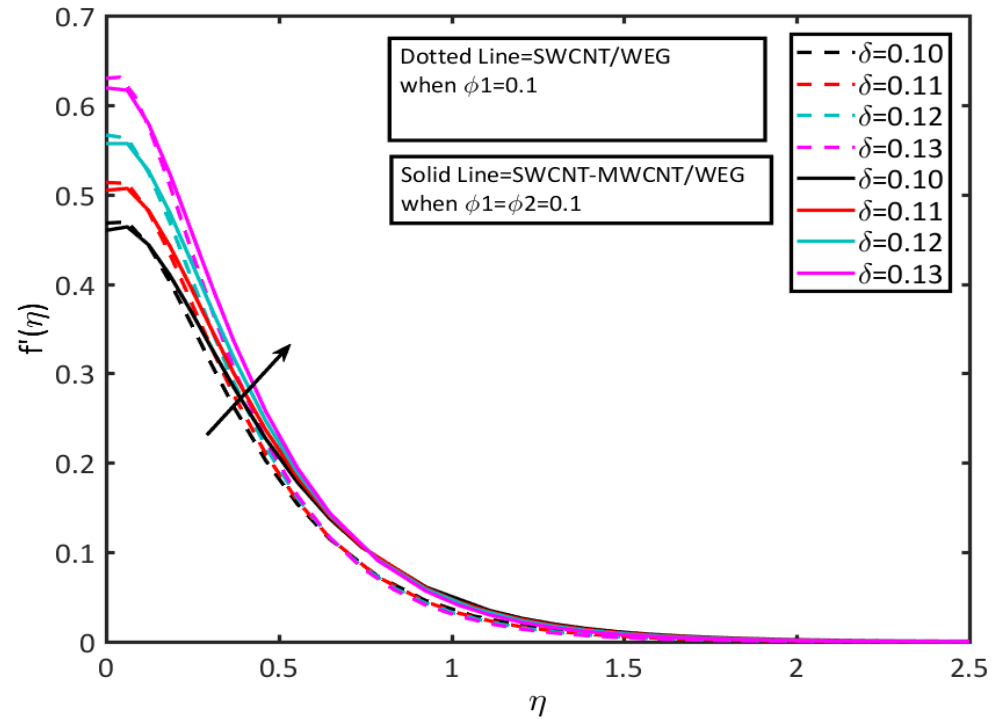

Fig. 3: Velocity profile f' for δ.

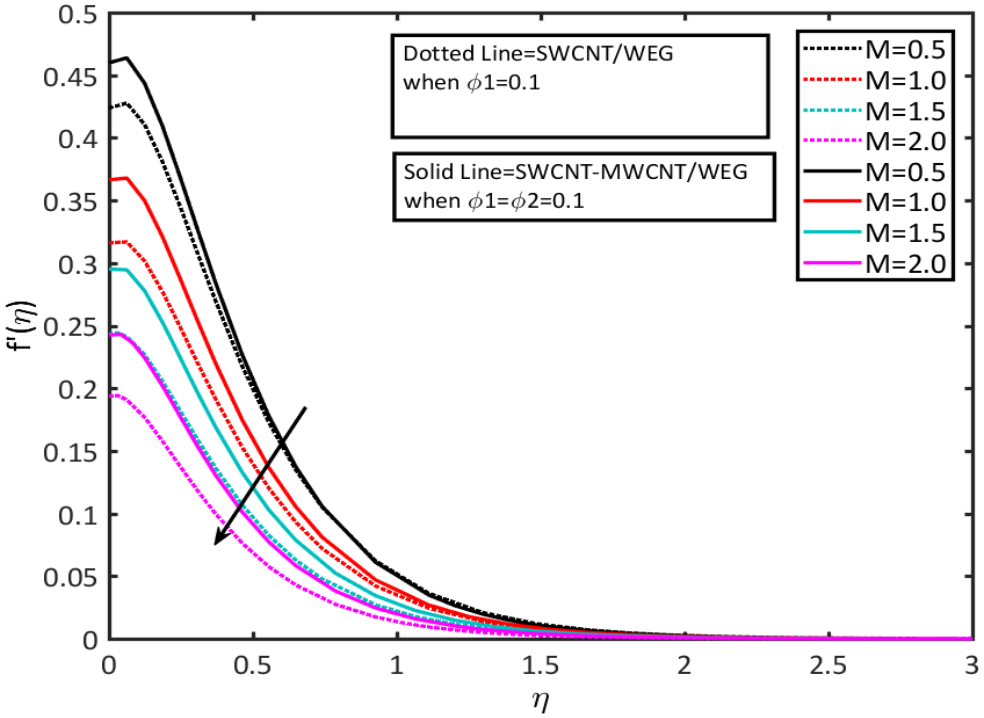

Fig. 4: Velocity profile f' for M.

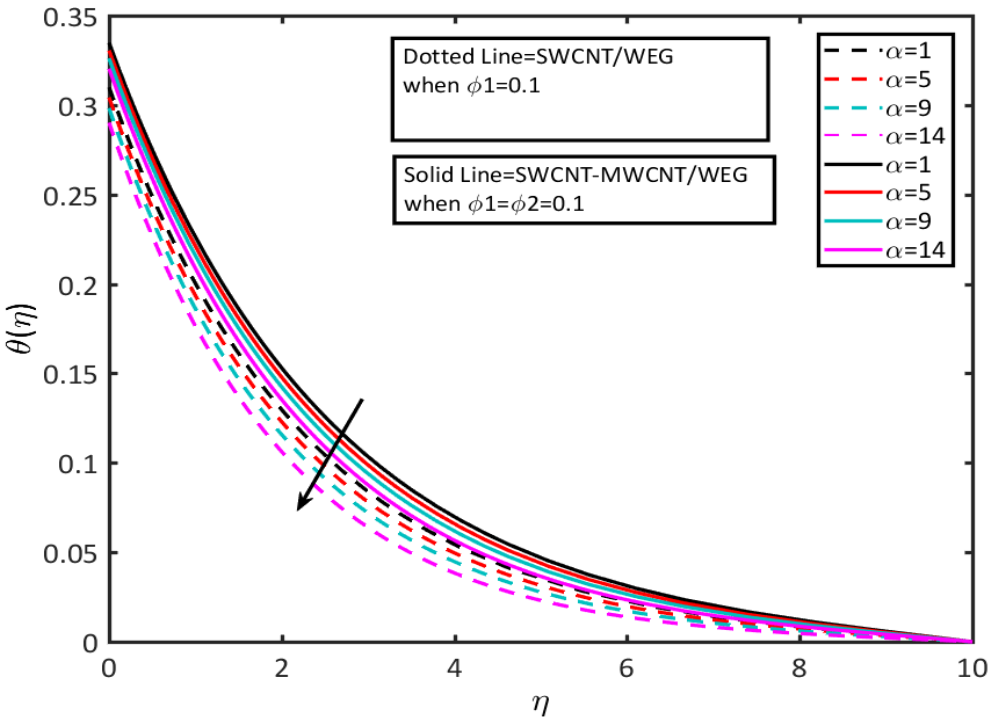

Fig. 5: Temperature profile θ for α.

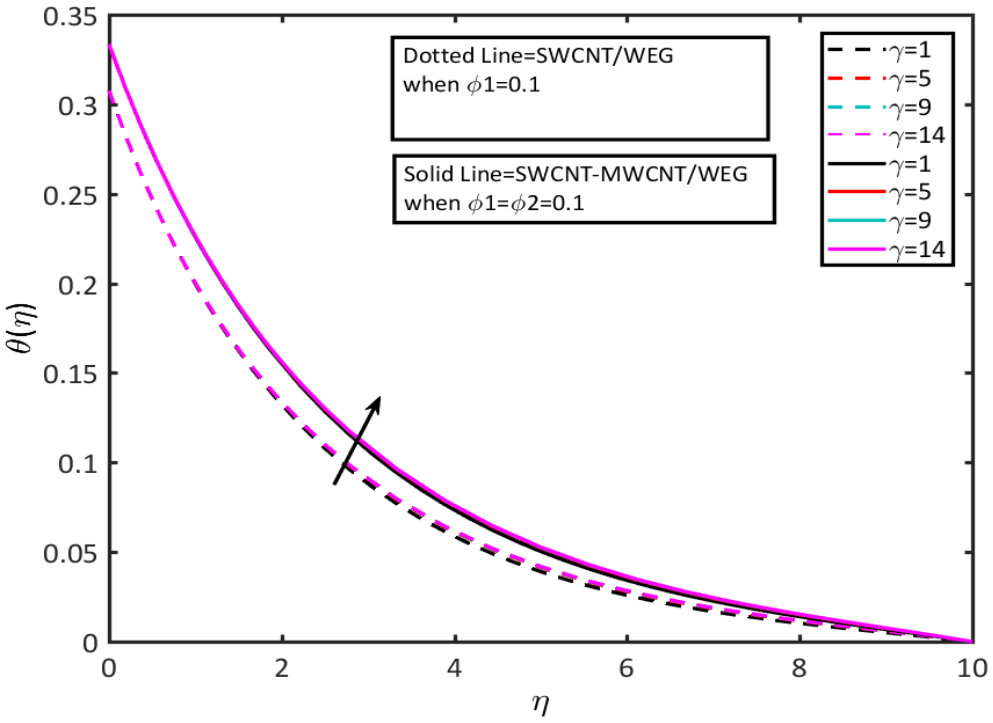

Fig. 6: Temperature profile θ for γ.

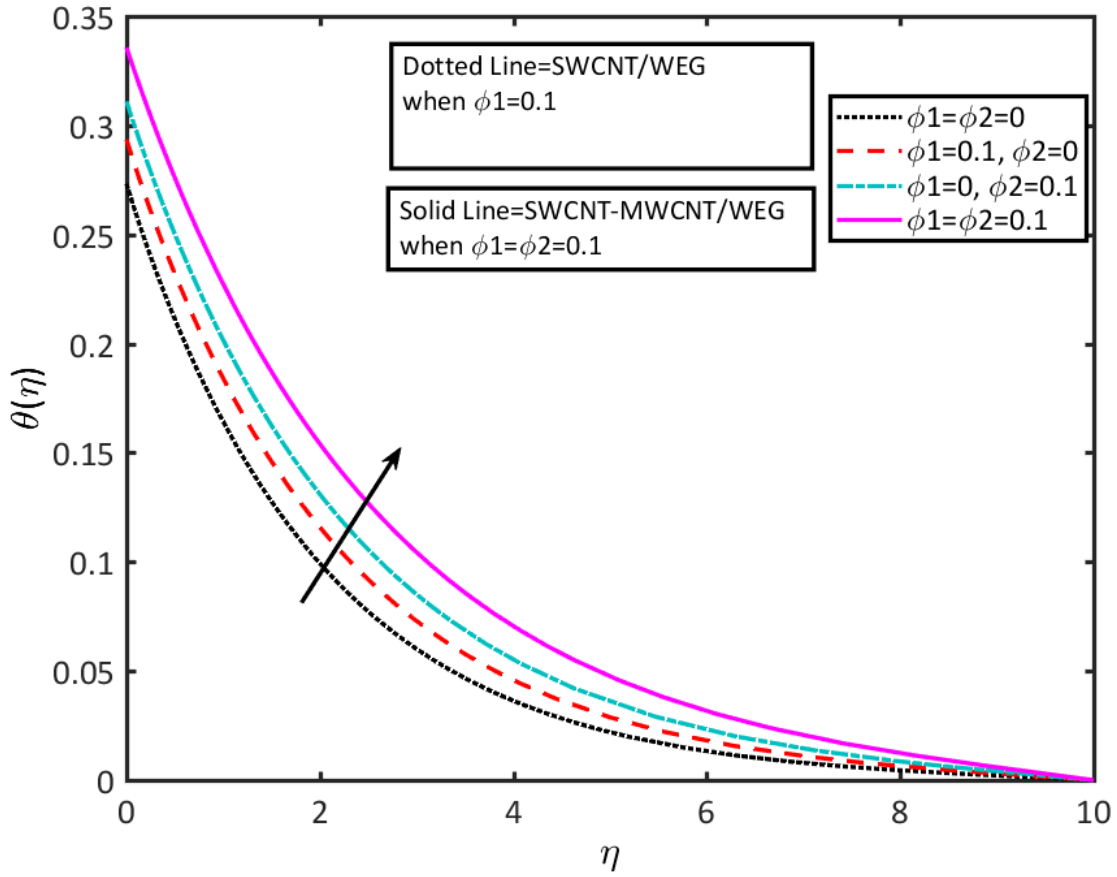

Fig. 7: Temperature profile θ for Casson fluid, Casson nanofluid and Casson hybrid nanofluid.

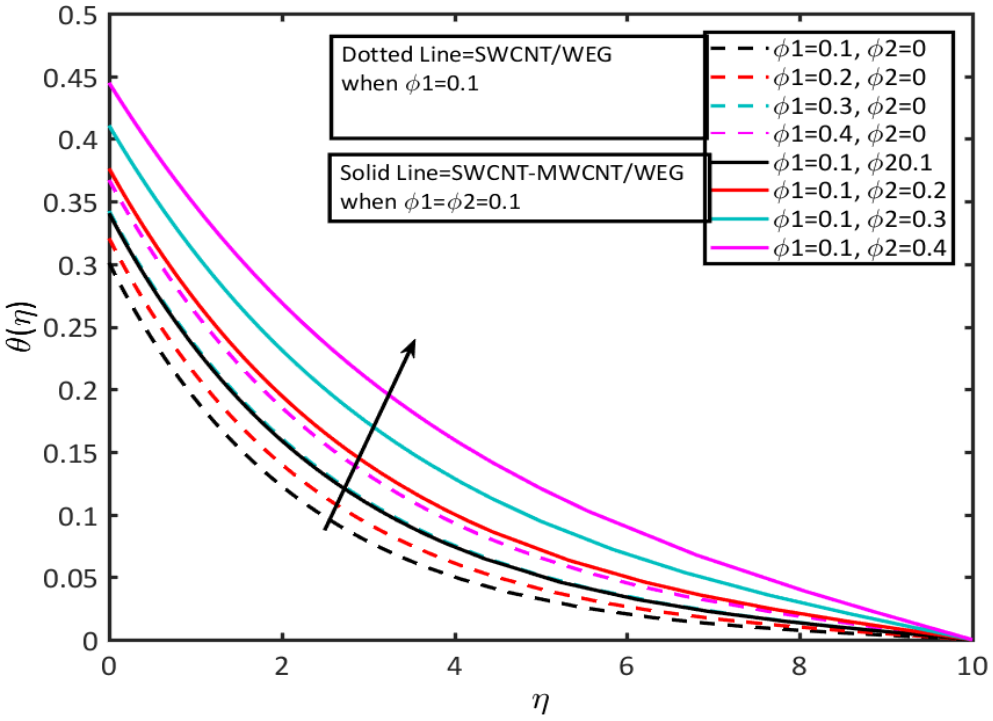

Fig. 8: Temperature profile θ for ϕ_1, ϕ_2.

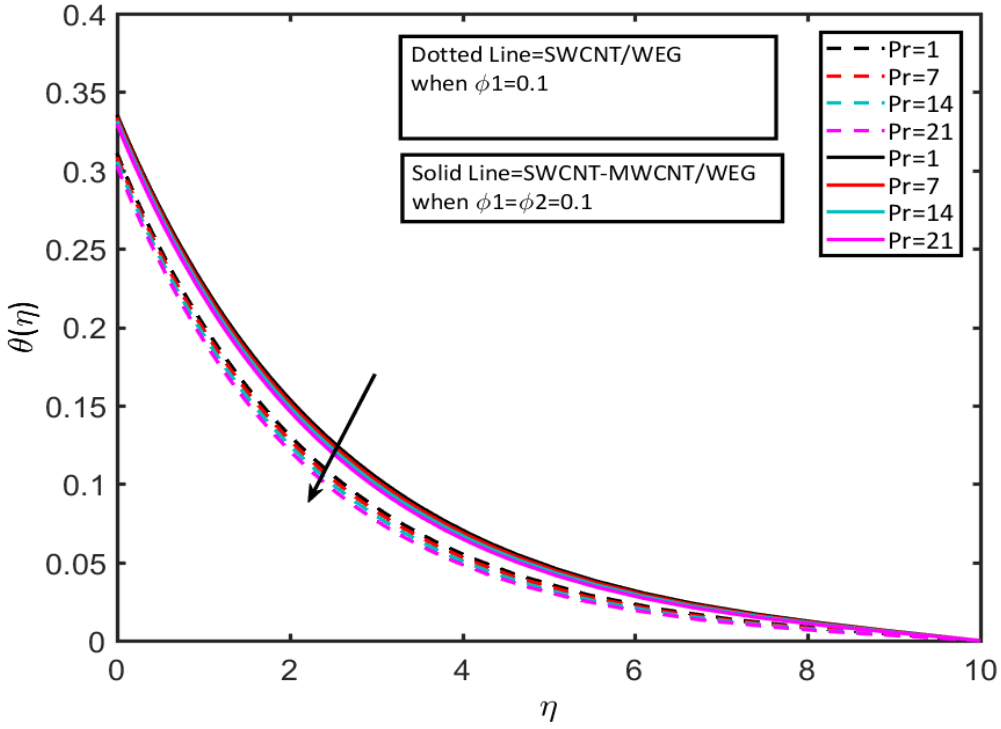

Fig. 9: Temperature profile θ for Pr.

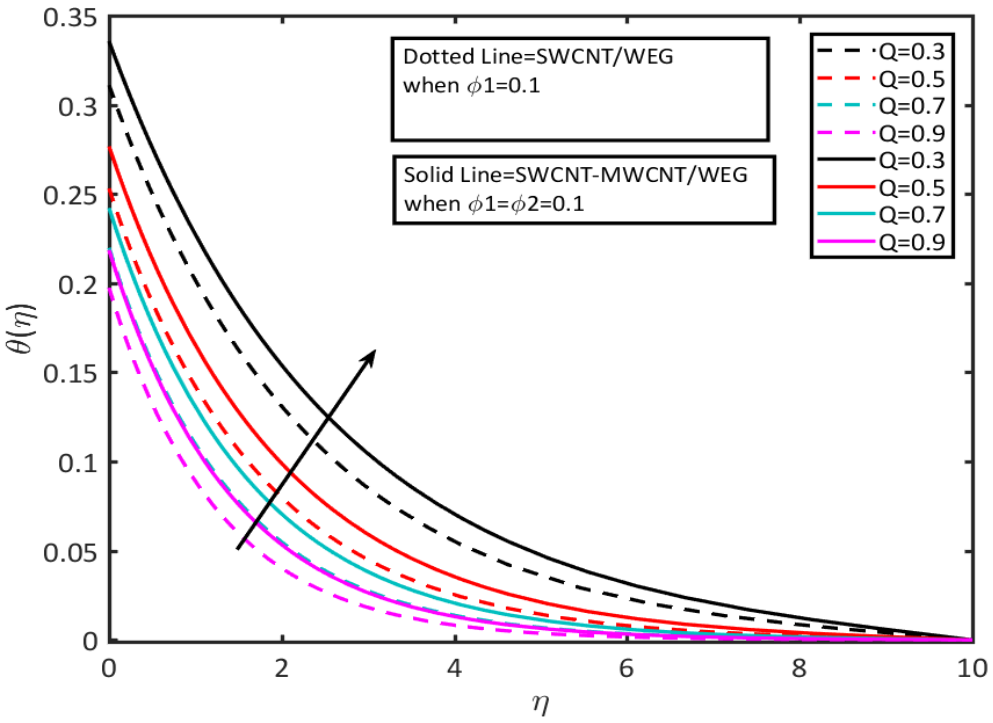

Fig. 10: Temperature profile θ for Q.

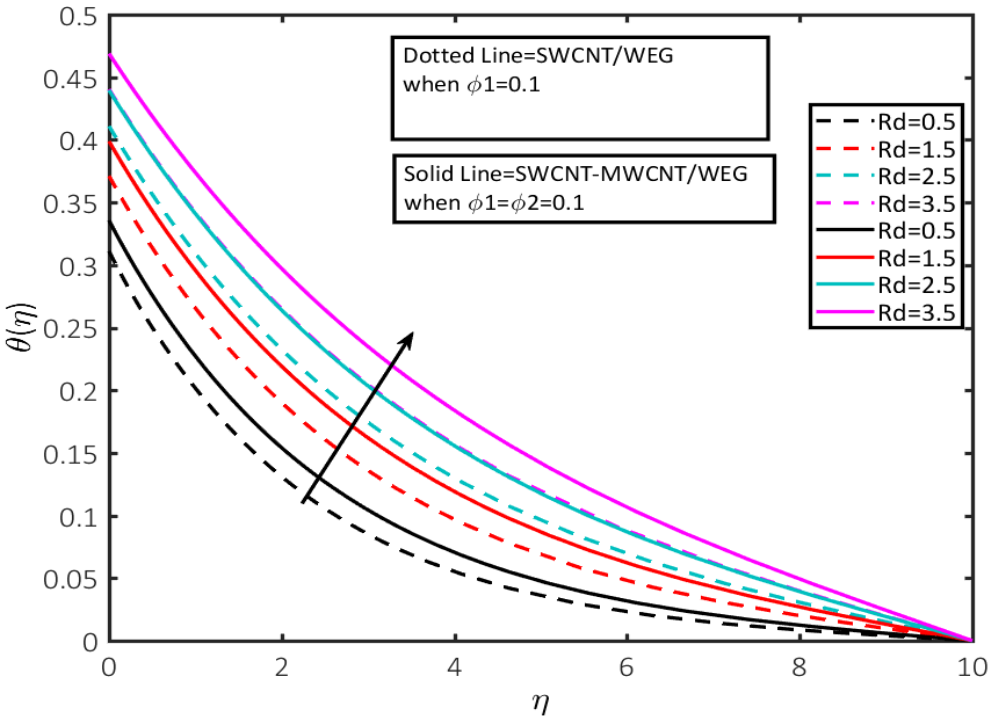

Fig. 11: Temperature profile θ for Rd.

Table 1: Thermal properties SWCNTs and MWCNTs with ethylene glycol base liquid.

Physical Properties	Ethylene Glycol (WE)	SWCNT	MWCNT
Density	1059.68	2600	1600
Specific Heat	335257	425	796
Thermal Conductivity	0.404	6600	3000
Electrical Conductivity	0.00276	10^6-10^7	1.9×10^{-4}

Table 2. Thermo-physical features of nanofluid (SWCNTs/EG) and hybrid nanofluids (SWCNTs-MWCNTs/WE) [5].

Properties	Hybrid nanofluid (SWCNT-MWCNT/WE)	Nanofluid (SWCNT/WE)
Electrical conductivity	$\frac{\sigma_{hnf}}{\sigma_f}=\frac{\sigma_{SWCNT}-2\phi_{SWCNT}\left(\sigma_{nf}-\sigma_{SWCNT}\right)+2\sigma_{nf}}{\sigma_{SWCNT}+\phi_{SWCNT}\left(\sigma_{nf}-\sigma_{SWCNT}\right)+2\sigma_{nf}}$ $\frac{\sigma_{nf}}{\sigma_f}=\frac{\sigma_{MWCNT}-2\phi_{SWCNT}\left(\sigma_f-\sigma_{MWCNT}\right)+2\sigma_f}{\sigma_{MWCNT}+\phi_{MWCNT}\left(\sigma_f-\sigma_{MWCNT}\right)+2\sigma_f}$	$\frac{\sigma_{nf}}{\sigma_f}=1+\frac{3(\sigma-1)\phi}{(\sigma+2)-(\sigma-1)\phi}$ $\frac{\sigma_s}{\sigma_f}=\sigma$
Viscosity	$\mu_{hnf}=\frac{\mu_f}{(1-\phi_{SWCNT})^{2.5}(1-\phi_{MWCNT})^{2.5}}$	$\mu_{nf}=\frac{\mu_f}{(1-\phi)^{2.5}}$
Heat capacity	$\left(\rho C_p\right)_{hnf}=\left(\rho C_p\right)_f(1-\phi_{SWCNT})\left[\begin{matrix}(1-\phi_{MWCNT}) \\ +\phi_{MWCNT}\frac{\left(\rho C_p\right)_{MWCNT}}{\left(\rho C_p\right)_f}\end{matrix}\right]$ $+\phi_{SWCNT}\left(\rho C_p\right)_{SWCNTs}$	$\left(\rho C_p\right)_{nf}=\left(\rho C_p\right)_f(1-\phi)+\phi\frac{\left(\rho C_p\right)_s}{\left(\rho C_p\right)_f}$
Density	$\rho_{hnf}=\rho_{SWCNT}\phi_{SWCNT}+\left[(1-\phi_{SWCNT})\left\{\begin{matrix}(1-\rho_{MWCNT})\rho_f \\ +\rho_{MWCNT}\phi_{MWCNT}\end{matrix}\right\}\right]$	$\rho_{nf}=\rho_s\phi+(1-\phi)\rho_f$

Thermal conductivity	$\frac{k_{hnf}}{k_f}=\frac{\left(k_{SWCNT}+(n-1)k_{nf}\right)-(n-1)\phi_{SWCNT}\left(k_{nf}-k_{SWCNT}\right)}{\left(k_{SWCNT}+(n-1)k_{hnf}\right)+\phi_{SWCNT}\left(k_{nf}-k_{SWCNT}\right)}$	$\frac{k_{nf}}{k_f}=\frac{\left(k_s+(n-1)k_f\right)-\phi\left(k_f-k_s\right)}{\left(k_s+(n-1)k_f\right)+\phi\left(k_f-k_s\right)}$

Table 3: Comparison of numerical results with study of Mustafa [26] taking $A=0,\ \phi_1=\phi_2=1$ and $\gamma\to\infty$.

Parameters		Mustafa [26]		Present results	
M	δ	$f'(0)$	$f''(0)$	$f'(0)$	$f''(0)$
0.0	0.25	0.064883	0.259534	0.064885	0.259535
0.2	0.25	0.047794	0.191176	0.047795	0.191177
0.4	0.25	0.036514	0.146057	0.036513	0.146056

Muapper Alhadri:

Muapper Alhadri is associate professor University of Ha'il, Ha'il City, Saudi Arabia. Dr. Alhadri has received PhD degree in mechanical engineering. His research expertise is in fluid mechanics and numerical analysis. Dr. Alhadri has published 36 research papers. He is also reviewer of many international journals.

Tasawar Abbas:

Dr. Tasawar Abbas is working in University of Wah, Wah Cantt, Pakistan., Pakistan. Dr. Abbas has published 40 research paper with impact factor 60 plus. His area of research is fluid mechanics and nanofluids. He is reviewer of 18 impact factor journals.

Sami Ullah Khan

Sami Ullah Khan is Associate Professor in the Namal University Mianwali Pakistan. Dr. Khan has published 370 research papers with impact factor 1000 plus. He is reviewer of more than 70 impact factor journal. Dr Khan is guest editor of 4 impact factor journals. Dr Khan has been awarded as distinguish researcher from university.

Lotfi Ben Said:

Lotfi Ben Said is working associate professor University of Ha'il, Ha'il City, Saudi Arabia. Dr. Said has received PhD degree in mechanical engineering. His research expertise is in mechanical and manufacturing engineeirng. Dr. Lotfi Ben Said has published 59 research papers. He is also reviewer of many international journals.

Walid Aich:

Walid Aich is Professor in the University of Hail, Saudia Arabia. Dr **Aich** is working in thermal systems and numerical analysis. Dr. Aich is author of 82 research articles. He is reviewer of more than 80 impact factor journals.

Lioua Kolsi:

Lioua Kolsi is an associate Professor in the University of Hail, Saudia Arabia. Dr Kolsi is working in thermal systems and published more than 300 research papers in different journals. His area of research is nanofluids, thermal engineering and computational fluid mechanics. Dr Kolsi is guest editor of applied sciences journal.

Huma Tayyab:

Huma Tayyab is working as a lecturer in the Department of Mathematics, University of Wah, Wah Cantt, Pakistan. She has completed in her MS in computation fluid mechanics in 2022. Her area of research is fluid mechanics and nanotechnology. She has published 5 research papers in different journal.